Red afterglow and luminescence arising from defects in CaS:Eu^{2+}, Tm^{3+}

Yoriko Suda[1,2], Yuki Tamura[2], Syota Yamaguchi[2], Yasushi Nanai[3] and Tsuyoshi Okuno[2]

[1] Department of Engineering, Tokyo University of Technology, Hachioji, Tokyo 192-0982, Japan
[2] Department of Engineering Science, The University of Electro-Communications, Chofu, Tokyo 182-8585, Japan
[3] Department of Materials Science and Engineering, National Defense Academy, Yokosuka, Kanagawa 239-8686, Japan

E-mail: h57924d8@edu.teu.ac.jp, sudayoriko@uec.ac.jp

Abstract

CaS:Eu^{2+}, Tm^{3+} is a phosphor known to emit a long afterglow of red emission (650 nm) when excited by blue light (450 nm). It shows a long afterglow time of 700 s for Eu = 0.05% and Tm = 2%. The mechanism of this afterglow is investigated using time-resolved fluorescence (TR-F) spectroscopy from the nanosecond to millisecond region. At room temperature, it is not possible to investigate shallow levels because of the effects of thermal vibrations. The mechanism of the emission characteristics at room temperature would be affected by these levels that can be observed only at low temperatures. Therefore, the samples are cooled to 15 K for the TR-F measurements. The host material CaS emits blue light (420 nm) arising from sulfur defects, and the typical decay time is measured to be 6 ms. This blue emission becomes stronger when Tm^{3+} is doped. Furthermore, the doped Eu ions emit a broad red spectrum at 650 nm originating from the Eu^{2+}-specific 4f^{6}5d^1–4f^7 transition. When the excitation is ceased, the red emission decays with a fast time constant of 0.6 µs. This value is a typical decay time for Eu^{2+}. This red emission has multiple decay time constants, and a component with a decay time of 6 ms appears. This 6-ms decay time is the same as that of the blue emission from the sulfur defects, which have an important role on the red afterglow.

Keywords: luminescence, afterglow, phosphor, sulfide, europium, time-resolved fluorescence, defect

1. Introduction

Long-afterglow phosphors are used not only for safety signage but also for many purposes in daily life such as soft illumination and luminescent tape sticker. Various types of phosphors have already been developed for these purposes. The most famous long-afterglow phosphor is SrAl$_2$O$_4$:Eu^{2+}, Dy^{3+} [1, 2]. Other materials such as Sr$_2$MgSi$_2$O$_7$:Eu^{2+}, Dy^{3+} [3] and CaAl$_2$O$_4$:Eu^{2+}, Nd^{3+} [4] are used; however, most long-afterglow phosphors emit in the green and blue regions. There

are also long-afterglow phosphors that emit red light, such as Y$_2$O$_2$S:Eu^{3+}, Ti^{4+}, Mg^{2+} [5], SnO$_2$:Sm^{3+}, Zr^{4+} [6], ZrO$_2$:Sm^{3+}, Sn^{4+} [7], and CaTiO$_3$:Pr^{3+}, Al^{3+} [8]. However, red afterglow with a practical brightness has not yet been obtained from these materials. Further, the excitation energy has been reduced for afterglow phosphors because the fluorescence light is replaced by white LED light. White LED does not contain UV light, and thus, sufficient brightness is not obtained from afterglow phosphors. The development of new

bright afterglow phosphors excited by visible light is highly demanded.

Eu^{2+} doped calcium sulfides co-doped with rare-earth ions (Tm^{3+}, Pr^{3+}, Dy^{3+}) are well known as high-intensity red phosphors [9-15]. These phosphors are also expected to be applied in biological imaging using long-afterglow and photostimulated red luminescence under near-infrared excitation [11, 12]. Recently, CaS:Eu^{2+}-based phosphors have received renewed attention because they can be excited by blue-LED light. The authors reported that CaS:Eu^{2+}, Tm^{3+} showed a long afterglow even with blue excitation [16]. The high-brightness phosphor can be obtained by firing CaS in an iodine (I$_2$) atmosphere. For Eu=0.05% and Tm=2%, the afterglow of 700 s was observed in the red emission of 650 nm. The CaS:Eu^{2+} phosphor emits the red light via the 4f^{6}5d^1–4f^7 transition of Eu^{2+}. Usually, the decay time of CaS:Eu^{2+} is ~1 μs [17, 18]. The afterglow on a millisecond or second time region is too long for Eu^{2+} emission. It is assumed that this long afterglow is the emission of electrons temporarily trapped in defect levels of the host crystal. SrAl$_2$O$_4$:Eu^{2+}, Dy^{3+} is well known as a green long-afterglow phosphor. The afterglow of the Eu^{2+} emission in SrAl$_2$O$_4$:Eu^{2+}, Dy^{3+} is prolonged by electrons trapped in host defects of O^{2-} vacancies [1, 2].

To improve the characteristics of the afterglow, it is necessary to clarify the emission mechanism. The authors have reported that the millisecond-scale afterglow of nitride phosphors arises from nitrogen defects [19-21]. This was investigated using the time-resolved fluorescence (TR-F) method. The TR-F measurement of the nanosecond–millisecond scale is suitable for investigating not only the emission characteristics of rare-earth ions but also the defects of the host crystal. The interaction between rare-earth ions and the defect states in the host crystals, and the energy transfer between them, can also be studied. In this study, we investigated the afterglow mechanism of CaS:Eu^{2+}, Tm^{3+} using the TR-F measurement.

2. Methods

Samples were prepared using the same method described in the [16]. CaS, EuS, Tm$_2$S$_3$, and iodine were placed in a quartz tube, which was evacuated to ~50 Pa and fired at 1100 °C for 24 h. The raw materials were purchased from Kojundo Chemical Laboratory, Japan. The atomic ratio of Ca:Eu:Tm was 1:x:2% (x = 0.01%–1%). Tm-doped CaS (CaS:Eu=0%, Tm=2%) and Eu-doped CaS (CaS:Eu=0.1%, Tm=0%) were also prepared. In addition, two types of undoped CaS were investigated. CaS denotes the as-purchased raw material. CaS:Eu=0%, Tm=0% denotes undoped CaS that was heat-treated in the same way in the quartz tube including iodine as for the other CaS:Eu, Tm samples.

X-ray diffraction (XRD; RINT2200–Ultima III, Rigaku, Japan) measurements were performed using Cu Kα_1 radiation. Diffuse reflectance spectra and the internal quantum efficiency were measured using a spectrophotometer (C11347-01, Hamamatsu Photonics, Japan) equipped with an integrating sphere. The excitation in this spectrophotometer was conducted with a xenon arc lamp (150 W). The internal quantum efficiency corresponds to the photon-number ratio of luminescence to absorption. Afterglow times were measured as described in the [16]. The afterglow time was defined as the time for the luminance to reach 0.32 mcd m^{-2} after ceasing of visible-light excitation for 10 min. This value is the lowest luminance that human eyes can see.

For thermoluminescence (TL) measurements, a high-pressure mercury lamp (254 nm) was used as the excitation source, and detection was conducted using a photomultiplier tube (R374, Hamamatsu Photonics, Japan). The sample was cooled to 70 K using a cryostat. The sample was irradiated for 30 min, and then, the light source was turned off using a shutter. The sample was left for 20 min to wait for the appearance of afterglow at 70 K. The TL intensity was measured while the sample was being heated to 600 K at a constant rate (5 K min^{-1}). The bias voltage for the photomultiplier tube was set to 580 V.

For the TR-F measurements, the fourth harmonic generation (266 nm) of a Nd:YAG laser (Ultra CFR, Big Sky Laser Technologies, Inc., MT, USA) was used as the excitation light source. The pulse duration of the laser was 10 ns, and the repetition rate was 10 Hz. Emission spectra were measured in synchronization with the laser pulse using a Spectra Pro 2300i monochromator and a PI-Max CCD detector (Princeton Instruments, NJ, USA). The glass filter UV-31 was used to cut off the excitation light source. The TR-F spectrum for each measurement was obtained by accumulating 30 times. The sample was cooled to 15 K and then heated to 300 K.

3. Results and discussion

3.1 Static properties and afterglow

The XRD patterns of the CaS:Eu^{2+}, Tm^{3+} samples are presented in Figure 1. In the lower part of the figure, the patterns of the powder diffraction files of CaS and Tm$_2$O$_3$ are shown. The crystal structure of CaS is face-centered cubic ($Fm\bar{3}m$ (no. 225)), and the lattice constant is a=5.68 Å. All the samples used in this study were confirmed to be CaS. Scanning electron microscopy (SEM) observation showed (see figure S1) that the heat treatment performed in this study resulted in well-crystallized CaS. For Tm-doped CaS, small traces of diffraction peaks corresponding to Tm$_2$O$_3$ appear at 29.5° and 49.5°, which may be due to the effect of residual oxygen in the evacuated quartz tube during the heating procedure. This finding suggests that the real concentration of Tm in the Tm-doped CaS is less than 2%. The small diffraction peaks of Tm$_2$O$_3$ did not correlate with the measurement results below in this paper.

Figure 2 presents the diffuse reflectance spectra of CaS, CaS:Eu=0%, Tm=0%, CaS:Eu=0%, Tm=2%, CaS:Eu=0.1%, Tm=0%, and CaS:Eu=0.1%, Tm=2% at 300 K. The band gap of the host crystal CaS is reported to be 5.0 eV (250 nm) to 5.3 eV (230 nm) [11, 22], and the absorption edge is not included in this measurement range. For CaS, the raw material as purchased, the reflectance decreases from 600 to 250 nm, which is considered to correspond to the absorption of intrinsic tail states below the band gap [11]. It is suggested that intrinsic S vacancies V_S in the CaS host matrix are included [11, 23-25]. Electron paramagnetic resonance (EPR) results also confirmed the presence of V_S (see figure S2). For CaS:Eu=0%, Tm=0% and CaS:Eu=0%, Tm=2%, similar reflectance spectra to that of CaS are shown in figure 2. For CaS:Eu=0.1%, Tm=0% and CaS:Eu=0.1%, Tm=2%, clear absorption of Eu^{2+} appears between 420 and 600 nm. This absorption corresponds to the transition from the ground $4f^7$ state to the upper $4f^6 5d^1$ state. It is apparent that visible blue light can be absorbed by Eu-doped CaS.

As is shown in figure S1, all of the signal intensities of V_S in EPR for the heat-treated samples were the same within twice that of CaS. The effect of V_S on the afterglow of Eu^{2+} and the interaction between V_S and Eu^{2+} will be discussed in this paper. Surface states in CaS may also influence the afterglow phenomenon. However, the diameter of the heat-treated samples (5-10 μm) are larger than that of CaS (0.5 μm), as was shown in figure S1. In addition, no apparent EPR signal for surface states is observed in figure S1(a). This situation is the same in the references of EPR studies for CaS phosphors [26-28]. Therefore, the effect of surface states on optical properties in our CaS:Eu^{2+}, Tm^{3+} samples is not discussed in this paper.

Figure 3 shows the Eu concentration dependence of (a) the internal quantum efficiency and (b) the TL peak intensity and the afterglow time. In the TL measurements, the peak temperature is related to the activation energy from the trap level to the conduction band, and the peak intensity is related to the concentration of electron traps. The TL peak was located at 270 K, and its full width at half maximum was 30 K. This TL peak intensity in figure 3(b) should be related to the afterglow phenomena at 300 K [16]. The internal quantum efficiency in figure 3(a) reaches the maximum of 60% for Eu=0.1% and remains 50% for Eu=1%. In contrast, the TL peak intensity reaches the maximum at Eu=0.05% and decreases for higher Eu concentrations. The afterglow time in figure 3(b) shows the same tendency as the Eu concentration dependence of the TL intensity. The maximum afterglow time is 700 s for Eu=0.05%. The afterglow time becomes shorter for higher Eu concentrations. The good correlation between the afterglow time and the TL intensity or the concentration of electron traps is demonstrated for CaS:Eu, Tm in figure 3(b).

3.2 TR-F measurements for Eu=0%

The time-dependent changes in emission spectra and decay characteristics were investigated using the TR-F measurements. Figure 4 presents (a) the time-resolved spectra on excitation laser pulses (the sampling time of 50 ns) and (b) the decay characteristics (the sampling time of 1 ns) measured at 15 K. The spectra in figure 4(a) are stored while the excitation laser having 10-ns pulse width appears. The samples are CaS, CaS:Eu=0%, Tm=0% and CaS:Eu=0%, Tm=2%. As shown in figure 4(a), CaS emitted light in the ultraviolet (350 nm) to blue (420 nm) region in the initial 50-ns time range of emission. The 350-nm emission is not discussed in this paper because the spectral shape is distorted by the excitation laser (266 nm) and the filter (UV-31). We assume that this luminescence is due to the tail state of the band edge.

For CaS:Eu=0%, Tm=2%, which is heat treated, the blue emission at 420 nm increases. The 420-nm blue emission is considered to be related to intrinsic S defects in the CaS host matrix [11]. The 420-nm blue emission includes a periodical structure, as shown in figure 4(a). The period is approximately 735 cm^{-1}, and this structure is also present for CaS. Thus, the periodical structure in the 420-nm blue emission instantaneously present in the initial 50-ns time range may be related to some vibration in the CaS host matrix. However, the origin of this periodical structure is currently unknown and left for future research. It is known that Tm^{3+} undergoes a transition from the $^1D_2$ to $^3H_6$ level at 370 nm [29]. This wavelength agrees with the short wavelength of the 420-nm emission band. The transition of Tm^{3+} may increase the 420-nm emission band.

In figure 4(b), all of the temporal profiles are approximately the same. The initial rising profiles of the emission intensity agree with the laser profile. The decay time of the emission in figure 4(b) is approximately 10 ns, which is the time resolution of this measurement. In figure 4, the 420-nm emission band due to intrinsic defects in the CaS host matrix instantaneously appears in the 50-ns time region. This means that the photoexcited carriers move to defect states in this time scale.

Figure 5 presents the results of TR-F measurements in the millisecond time range. The data in figure 5 are stored at 0.5 ms after the laser excitation. The samples are the same as those in figure 4. Figure 5(a) presents the time-resolved spectra (the sampling time of 0.05 ms). While the blue emission band is slightly shifted from 420 nm in figure 4(a) to 400 nm in figure 5(a), this emission band is preserved at 0.5 ms after the laser excitation. Figure 5(b) presents decay curves of the blue emission. All of the curves in figure 5(b) have the same slope, and the typical time constant between the 2-ms and 10-ms range is 6 ms. This emission of CaS is considered to appear from the defect level due to S vacancies (V_S) [11, 23-25]. The defect level acts as an electron trap, and the electrons excited in the conduction band are trapped in this level. They return to the conduction band using thermal phonons or directly emit

blue light to return to the ground state. The characteristic of emission through defects is considered to appear in figure 5(b). The 6-ms decay time appears in this time range, and a longer decay component may also appear for a longer time range.

As shown in figure 5(a), almost the same TR-F spectra were obtained for CaS and CaS:Eu=0%, Tm=0%. For CaS:Eu=0%, Tm=2%, line peaks of the Tm^{3+} transitions appear in addition to the blue emission at 400 nm. The peaks at 480 nm correspond to the $^1G_4$–$^3H_6$ transition, whereas those at 660 nm correspond to the $^1G_4$–$^3F_4$ or $^1D_2$–$^3H_4$ transition of Tm^{3+} [29-32]. The decay curves of the line peaks of Tm^{3+} are the same as those of the blue emission in figure 5(b). It is suggested that the transitions of Tm^{3+} interact with the defect levels in the CaS host matrix.

3.3 TR-F measurements for Eu=0.1%

Eu^{2+}-doped samples were investigated, and the effect of the Tm^{3+} doping was studied. Figure 6 presents (a) the time-resolved spectra on excitation laser pulses (the sampling time of 50 ns) and (b) the decay characteristics (the sampling time of 1 ns) at 15 K. The samples were CaS:Eu=0.1%, Tm=0% and CaS:Eu=0.1%, Tm=2%. In figure 6(a), two broad emission bands are observed at 420 and 650 nm. The 650-nm red emission is due to the $4f^65d^1$–$4f^7$ transition of Eu^{2+}. This 650-nm red emission is stronger for CaS:Eu=0.1%, Tm=0% than for CaS:Eu=0.1%, Tm=2%.

The 420-nm blue emission is considered to be the same for Eu=0% in figure 4(a) and is related to intrinsic S defects in the CaS host matrix [11]. In figures 6(a) and (b), the 420-nm blue emission is stronger for CaS:Eu=0.1%, Tm=2% than for CaS:Eu=0.1%, Tm=0%. This situation is the opposite for the 650-nm red emission. The decay profiles of the 420-nm blue emission in figure 6(b) are almost the same as the excitation laser profile, as in the case in figure 4(b). In contrast, the 650-nm red emission of Eu^{2+} does not decay at all in this time region. It should be noted that the 650-nm red emission increases instantaneously within 10 ns. The profiles of the 650-nm red emission of CaS:Eu=0.1%, Tm=0% and CaS:Eu=0.1%, Tm=2% are the same in figure 6(b).

Figure 7(a) presents the time-resolved spectra at 0.5 ms after the laser excitation (the sampling time of 0.05 ms). In figure 7(a), the 650-nm red emission is stronger for CaS:Eu=0.1%, Tm=2% than for CaS:Eu=0.1%, Tm=0%. This is the opposite in figure 6(a) (the sampling time of 50 ns). The red emission in the long time region is increased by the Tm doping. Figure 7(b) presents the decay curves in the 10-ms time range. The intensity of the 650-nm emission for CaS:Eu=0.1%, Tm=0% decreases more rapidly than for CaS:Eu=0.1%, Tm=2% in this time range. The 420-nm blue emission is also observed in figure 7(b); the emission intensity is weak compared with the 650-nm red emission. In figure 7(b), the emission of CaS:Eu=0.1%, Tm=2% is stronger than that of CaS:Eu=0.1%, Tm=0% both at 420 and 650 nm. The

intensity of the 420-nm blue emission for CaS:Eu=0.1%, Tm=0% is quite small and less than the background of this measurement. The decay profiles of the other three emissions in figure 7(b) are almost the same, with a typical decay time constant of 6 ms in the time range between 2 and 10 ms. This value is the same as that for CaS:Eu=0% in figure 5(b). This decay time is supposed to reflect the decay time of the defect level transition of the CaS host crystal. The decay time of the $4f^65d^1$–$4f^7$ transition of Eu^{2+} is often reported to be approximately 1 µs [17, 18]. The decay time (6 ms) of the 650-nm red emission in figure 7(b) is not determined by the Eu^{2+} transition itself but by the defect-level transition of the CaS host crystals. The electrons trapped by the defect level move to Eu^{2+} and emit red light at 650 nm. In this manner, the 650-nm red emission of Eu^{2+} decays with the same time constant as the 420-nm blue emission of the defect.

In some of the references [23, 24] on CaS:Eu^{2+} phosphors, emission from Eu^{3+} was reported. However, for the samples in this paper, no emission of Eu^{3+} is detected as is shown in figure S3. In Eu^{2+}-doped nitride phosphors, emission of Eu^{3+} locating at surfaces of the phosphor particles is reported [33]. In this paper, the size of the particles is enlarged by the heat treatment, as was shown in figure S1. The effect of the surface is considered to be negligible and Eu^{3+} is not involved in the optical properties of the CaS:Eu^{2+}, Tm^{3+} phosphors in this paper.

3.4 Effects of Eu concentration

The effect of the Eu^{2+} concentration on the emission spectrum and decay characteristics in the 0.01-ms time range was investigated. Figure 8(a) presents the time-resolved spectra on excitation laser pulses (the sampling time of 50 ns). The samples were CaS:Eu=0.01% ~ 1%, Tm=2%. The measurement temperature was 15 K. Two broad emission peaks are observed at 420 and 650 nm, as in figures 6(a) and 7(a). The 420-nm blue emission decreases with increasing the Eu concentration. The absorption band by Eu^{2+} was observed at approximately 450 nm in figure 2, and thus, reabsorption or the energy transfer to Eu^{2+} occurs. Therefore, the 420-nm blue emission of the defect levels is reduced.

The intensity of the 650-nm red emission is the maximum for CaS:Eu=0.05%, Tm=2% and decreases with increasing the Eu concentration. Figures 8(b) and (c) show the decay characteristics of the 650-nm red emission and the 420-nm blue emission in the 0.01-ms time range. In figure 8(b) for CaS:Eu=0.01%, Tm=2% with the low Eu^{2+} concentration, the 650-nm red emission decays to ~ 4 µs in a straight line, and the time constant calculated from the slope is 0.6 µs. This is similar to the reported value of the Eu^{2+} transition [17, 18]. The intrinsic decay time constant of Eu^{2+} in CaS appears in figure 8(b). After 4 µs in figure 8(b), the 650-nm red emission decays with the same slope as that for the 420-nm blue emission. In figure 8(c) for CaS:Eu=1%, Tm=2% with the

high Eu^{2+} concentration, the 650-nm red emission decays with a time constant of 0.6 μs and disappears at 7 μs. The 420-nm blue emission decreases rapidly and disappears at 2 μs. In figure 8(c), both of the 650-nm red emission and the 420-nm blue emission disappear after 7 μs, and both of the emissions have the same decay slope in figure 8(b). The Eu^{2+} emission at 650 nm is affected by the defect emission at 420 nm, and Eu^{2+} and the defect level interact with each other.

3.5 Effects of temperature

Figure 9 shows the temperature dependence of the TR-F spectra of CaS:Eu=0.01%, Tm=2% between 12 K and 300 K. The longer sampling time of 500 ns than 50 ns in figure 8 is used, in order to detect clearly the small emission intensity at high temperatures such as 300 K. In the ultraviolet and blue regions, the emission intensity is strong at 12–25 K and the 420 nm peaks are clear. The emission intensity decreases with increasing the temperature. The line peaks in this wavelength region correspond to Tm^{3+}. The peaks at 370 nm ($^1D_2$–$^3H_6$) and 470 nm ($^1D_2$–$^3F_4$) [23-26] are strong at 125 K. As the temperature increases to 200 K, the emission at 370 nm and 470 nm becomes weak and the emission at 480 nm ($^1G_4$–$^3H_6$) becomes strong [30]. The intensities of these emission bands decrease as the temperature increases.

The red emission of Eu^{2+} at 650 nm is strong at 50 and 75 K, and the intensity of the emission decreases with increasing the temperature. From 12 to 75 K, the line peak due to the zero phonon line of Eu^{2+} (625 nm) and its phonon shifts are observed [23, 25]. Above 100 K, the line peaks on the longer-wavelength side of the spectrum decrease. The emission spectrum becomes close to a symmetric profile and the central wavelength decreases.

The temperature dependence of the intensity at 420 and 650 nm is shown in figure 10. In figure 10, the intensity obtained in figure 9 for CaS:Eu=0.01%, Tm=2% is plotted. The blue emission at 420 nm is quenched by the increase in the temperature, and the emission intensity decreases to 35% of 12 K at 300 K. The red emission at 650 nm is stronger at 50 and 75 K than at 12 K. It is considered that phonons enhance the supply of electrons from the defect level of the host crystal to Eu^{2+}. Above 100 K, the luminescence intensity decreases rapidly to 15% of 12 K at 300 K. The overall tendencies of the blue emission at 420 nm and the red emission at 650 nm against the temperature are similar in figure 10. This is due to the interaction between the defect level for the blue emission and Eu^{2+} for the red emission.

The emission decay characteristics at 15 K and 300 K for CaS:Eu=0.1%, Tm=2% are presented in figure 11. The decay curves of the 420-nm blue emission and the 650-nm red emission are shown in the figure. At 15 K, the 420-nm blue emission is recognized between 0 and 10 ms in figure 11 (the data in figure 7(b) are plotted again). However, the blue emission decreases rapidly at 300 K and disappears at 0.5 ms. The blue emission is quenched at 300 K.

The 650-nm red emission due to Eu^{2+} is affected by the defect levels, which is the origin of the 420-nm blue emission. The depth of the defect levels from the conduction band is considered to have some inhomogeneous distribution. The average depth was estimated to be 0.3 eV using the Hoogenstraaten method for the TL glow peak in the [16]. The depth of the defects contributing to the 650-nm red emission changes depending on the temperature. This situation is reflected in the decay profiles of the 650-nm red emission in figure 11. The decay component of the 650-nm red emission is stronger at 15 K than at 300 K between 0 and 5 ms in figure 11. The decay time in the time region between 2 and 10 ms at 15 K was determined to be 6 ms in figure 7(b). This decay component is not observed for the decay curve at 300 K. After 5 ms, the 650-nm red emission is stronger at 300 K than at 15 K. The 6-ms decay component in the 650-nm red emission is reduced because of the temperature quenching of the 420-nm blue emission at 300 K. From the slope between 5 and 10 ms for 650 nm at 300 K in figure 11, the decay time is longer in this time region. The decay time is estimated to be 20 ms. Even at 10 ms, the 650-nm red emission remains. The decay time of luminescence from defects changes depending on the measurement time region. It is observed that a longer decay time than milliseconds is present [16]. This longer decay time causes the 700-s afterglow in figure 3(b).

The time-integrated luminescence due to defect levels at 420 nm is quenched at 300 K. This means that the defect level contributing to the blue emission is quite close to the conduction band. Figure 12 presents the TL glow curves (the heating ramp rate of 5 K min^{-1}). There is no glow peak in CaS (the raw material). The heat-treated sample of CaS:Eu=0%, Tm=0% has peaks at 100 K and 200–300 K. The peak at 100 K disappears, and a peak at 400 K appears for CaS:Eu=0%, Tm=2%. For the Eu-doped samples, the peak is observed only at 200–300 K. CaS:Eu=0.1%, Tm=0% has a peak at 240 K, and the peak of CaS:Eu=0.1%, Tm=2% is changed to the high temperature of 280 K. The peak temperature represents the depth of the trap level from the conduction band. The energy state is changed by doping with Tm and Eu, which changes the electron coordination around the defect. The glow intensity of co-doped CaS:Eu=0.1%, Tm=2% is much larger than that of the other samples. This defect level should cause the long afterglow of 700 s.

3.6 Afterglow and effects of Eu^{2+}

Figure 13 presents the energy diagram obtained from the experimental results in the preceding subsections. The band gap between the valence band and the conduction band of CaS of the host crystal is 5.3 eV. In figure 13(a), electrons are supplied to the conduction band by the laser excitation. Even if the energy of the laser is smaller than the band gap, the

electron is considered to be excited to the conduction band through tail states most likely present slightly below the band gap [11]. In CaS:Eu=0%, Tm=0%, electrons are trapped in the defect levels created by V_S, and some of them emit blue light at 420 nm (figure 13(c)). The typical decay time of the blue emission is 6 ms (figures 5(b) and 7(b)), and the decay profile includes multiple decay times. The carrier density is increased by including trivalent ions such as Tm^{3+} in CaS because Tm^{3+} replaces Ca^{2+} and creates charge defects [9-16].

In the [9], luminescence spectra of $CaS:Eu^{2+}$, Tm^{3+} were studied. The 420-nm blue emission was not observed and thus not considered. It was proposed that Tm^{3+} captures electrons and the electrons are supplied directly to Eu^{2+} from Tm^{3+} [9]. In our investigation using TR-F, Tm^{3+} increases the 420-nm blue emission of CaS even without Eu^{2+} doping (figure 4(a)). We consider that Tm^{3+} delivers electrons to the defect level V_S. Doping with Tm^{3+} enhances the blue emission of CaS at 420 nm (figures 4 and 6), and some sharp luminescence lines of Tm^{3+} appear (figure 13(b)). The excited state of Tm^{3+} gives electrons to the V_S level in figure 13(c) and increases the blue emission. In figure 13(d), doping of Eu^{2+} into CaS causes the broad 650-nm red emission (figures 6 and 7). This red emission appears by the direct excitation from the ground $4f^7$ state of Eu^{2+}, the supply of the electron from the conduction band of CaS, and the supply from the upper state of the 420-nm blue emission. The initial time constant of the 650-nm red emission is determined to be 0.6 μs (figures 8(b) and (c)). When the laser excitation is ceased, the electrons trapped in the upper state of V_S gradually move to Eu^{2+} thermally or through tunneling. This thermal activation or tunneling from the upper state of V_S to Eu^{2+} is the origin of the long afterglow, such as 700 s in figure 3(b) [16].

In figures 7(b) and 8(b), the slope of the decay curve for the 650-nm red emission is the same as that for the 420-nm blue emission. The trap level and the Eu^{2+} excited level ($4f^65d^1$) are thought to be located at approximately the same energy. They are considered to interact with each other. Because the electrons can move to both of the levels, the intensity of the 420-nm blue emission changes depending on the Eu^{2+} concentration (figure 8(a)). The 420-nm blue emission is quenched at room temperature (figures 8–10), which indicates the presence of shallow traps.

Figure 13(e) shows the mechanism of the afterglow after the excitation is ceased. For low Eu^{2+} concentration such as 0.05% in figure 3(b), electrons are trapped in several upper levels of V_S. An electron moves to the neighboring Eu^{2+} ion in a time scale, and several time scales are assumed to be present for one Eu^{2+} ion. The 650-nm red emission of Eu^{2+} under the effect of V_S in figure 13(e) has various decay times of 6 ms at 15 K (figures 7(b) and 8(b)), 20 ms at 300 K (figure 11), or 700 s at 300 K (figure 3(b)). For higher Eu^{2+} concentration such as 1% in figure 3(b), the number of V_S is smaller for one Eu^{2+} ion. V_S levels having an appropriate storage time for the

electron and an appropriate distance from Eu^{2+} are insufficient, and thus the afterglow is reduced.

It is suggested that the electron capture at the V_S defect level of the host crystal contributes to the appearance of the long red afterglow. The afterglow of Eu^{2+} was increased by the Tm^{3+} doping because electrons supplied to V_S was increased. This is consistent with the fact that the extension of the afterglow time has been reported for trivalent ions such as Tm^{3+}, Dy^{3+}, Pr^{3+}, and Sm^{3+} [7-16].

Recently, the authors reported the appearance of the blue emission of nitrogen defects and the green emission of Eu^{2+} for the β-SiAlON:Eu^{2+} green phosphor [21]. The interaction between the nitrogen defects and Eu^{2+} and the effect of the defects on Eu^{2+} were clearly observed by the TR-F and EPR measurements. These situations are quite similar to those discussed in this paper for $CaS:Eu^{2+},Tm^{3+}$. For β-SiAlON:Eu^{2+}, the density of defects located at approximately 0.3 eV, which would be suitable for long afterglow at 300 K, was quite small [21]. This would be desirable for the green phosphor for the usage of fast on–off switching of the green light. For $CaS:Eu^{2+},Tm^{3+}$, the density of defects located at 0.3 eV (figure 13(c)) is large, and thus, the promising red long afterglow is present [16]. The TR-F measurement at 300 K and low temperature is an effective method to monitor the defect levels, which largely affect the main emission band and are possibly detected only at low temperature or near the time origin of the laser excitation.

4. Conclusions

CaS:Eu=0.05%, Tm=2% has a red emission band at 650 nm and a long afterglow time of 700 s. The mechanism of this red long afterglow was investigated using TR-F spectroscopy. CaS has defect levels arising from S defects (V_S), which emit blue light at 420 nm (the typical decay time of 6 ms). Tm^{3+} increased this 420-nm emission. Eu^{2+} was excited by ultraviolet or blue light and emitted broad red emission of $4f^65d^1$–$4f^7$ at 650 nm. When the excitation light was ceased, the electrons trapped in the V_S level gradually moved to the upper $4f^65d^1$ state of Eu^{2+}, and the afterglow of 650 nm appeared. The decay curve of the red afterglow was the same as that of the blue emission. The blue emission from the defect levels was quenched by increasing the temperature or the concentration of Eu. The blue emission decreased with increasing the concentration of Eu, and the red afterglow due to Eu^{2+} also decreased. The electron trapped in the V_S defect level affected the luminescence properties of Eu^{2+} and the afterglow.

Acknowledgements

References

[1] Matsuzawa T, Aoki Y, Takeuchi N and Murayama Y 1996 A new long phosphorescence phosphor with high brightness, $SrAl_2O_4$:Eu^{2+},Dy^{3+} *J. Electrochem. Soc.* **143** 2670-3

[2] Liepina V, Millers D and Smits K 2017 Tunneling luminescence in long lasting afterglow of $SrAl_2O_4$: Eu, Dy *J. Lumin.* **185** 151-4

[3] Lin Y, Tang Z, Zhang Z, Wang X and Zhang J 2001 Preparation of a new long afterglow blue-emitting $Sr_2MgSi_2O_7$-based photoluminescent phosphor *J. Mater. Sci. Lett.* **20** 1505-6

[4] Teng X, Zhuang W, Hu Y, Zhao C, He H, Huang X 2008 Effrct of flux on the properties of $CaAl_2O_4$:Eu^{2+}, Nd^{3+} long afterglow phosphor *J. Alloys Compd.* **458** 446-9

[5] Wang X, Zhang Z, Tang Z and Lin Y 2003 Characterization and properties of a red and orange Y_2O_2S-based long afterglow phosphor *Mater. Chem. Phys.* **80** 1-5

[6] Zhang J, Ma X, Qin Q, Shi L, Sun J, Zhou M, Liu B and Wang Y 2012 The synthesis and afterglow luminescence properties of a novel red afterglow phosphor: SnO_2:Sm^{3+}, Zr^{4+} *Mater. Chem. Phys.* **136** 320-4

[7] Zhao Z and Wang Y 2012 The synthesis and afterglow luminescence properties of a novel red afterglow phosphor: ZrO_2: Sm^{3+}, Sn^{4+} *J. Lumin.* **132** 2842-6

[8] Nanai Y, Igarashi A and Kamioka H 2019 Excitation energy dependence for electron traps in $CaTiO_3$: Pr, Al single crystals *J. Phys.: Conf. Ser.* **1220** 012011

[9] Jia D, Jia W, Evans D R, Dennis W M, Liu H, Zhu J and Yen W M 2000 Trapping processes in CaS:Eu^{2+},Tm^{3+} *J. Appl. Phys.* **88** 3402-7

[10] Kojima Y, Aoyagi K and Yasue T 2007 Afterglow mechanism and thermoluminescence of red-emitting CaS:Eu^{2+}, Pr^{3+} phosphor with incorporated Li^+ ion upon visible light irradiation *J. Lumin.* **126** 319-22

[11] Rodriguez Burbano D C, Sharma S K, Dorenbos P, Viana B and Capobianco J A 2015 Persistent and photostimulated red emission in CaS:Eu^{2+}, Dy^{3+} nanophosphors *Adv. Opt. Mater.* **3** 551-7

[12] Gao Y, Li R, Zheng W, Shang X, Wei J, Zhang M, Xu J, You W, Chen Z and Chen X 2019 Broadband NIR photostimulated luminescence nanoprobes based on CaS: Eu^{2+}, Sm^{3+} nanocrystals *Chem. Sci.* **10** 5452-60

[13] Kong M, Fang M, Tan X, Liu M, Shang G L, Fei G T and Zhang L 2018 The investigation on the mechanism of the increased decay time in red SrS: Eu^{2+}, Dy^{3+} phosphor *Mater. Chem. Phys.* **207** 161-6

[14] Chen D, Xu W, Li X, Zhou Y, Liu S and Chen Y 2017 Near-infrared photo-stimulated red luminescence in Eu^{2+}/Ln^{3+} (Ln= La-Lu): SrS persistent phosphors *J. Alloys Compd.* **720** 239-44

[15] Du Jiaren, and Dirk Poelman 2020 Red-Light-Activated Red-Emitting Persistent Luminescence for Multicycle Bioimaging: A Case Study of CaS: Eu^{2+}, Dy^{3+} *J. Phys. Chem. C* **124** 16586-95

[16] Tamura Y, Okuno T, Suda Y and Nanai Y 2020 Red persistent luminescence excited by visible light in CaS: Eu^{2+}, Tm^{3+} *J. Phys. D: Appl. Phys.* **53** 155101

[17] Yen W M, Shionoya S and Yamamoto H (ed) 2007 *Phosphor handbook* 2nd edn (Boca Raton, FL: CRC Press)

[18] Poort S H M, Meyerink A and Blasse G 1997 Lifetime measurements in Eu^{2+}-doped host lattices *J. Phys. Chem. Solids* **58** 1451-6

[19] Suda Y, Kamigaki Y and Yamamoto H 2018 Blue emission in photoluminescence spectra of the red phosphor $CaAlSiN_3$: Eu^{2+} at low Eu^{2+} concentration *J. Appl. Phys.* **123** 161542

[20] Suda Y, Kamigaki Y, Miyagawa H, Takeda T, Takahashi K and Hirosaki N 2020 Luminescence and afterglow due to defects in β-SiAlON crystal powder *J. Phys. D: Appl. Phys.* **53** 165108

[21] Suda Y, Kamigaki Y, Miyagawa H, Takeda T, Takahashi K and Hirosaki N 2021 Effects of Eu^{2+} on the luminescence and afterglow that arise from defects in β-SiAlON: Eu^{2+} *J. Phys. D: Appl. Phys.* **54** 065102

[22] Kaneko Y and Koda T 1988 New developments in IIa–VIb (alkaline-earth chalcogenide) binary semiconductors *J. Cryst. Growth* **86** 72-8

[23] Yamashita N, Fukumoto S, Ibuki S and Ohnishi H 1993 Photoluminescence of Eu^{2+} and Eu^{3+} centers in CaS: Eu, Na phosphors *Japan. J. Appl. Phys.* **32** 3135-9

[24] Fukumoto S, Hayashi Y, Ibuki S, Abe K and Ohnishi H 1993 Photoluminescence of Eu^{2+} and Eu^{3+} centers in CaS: Eu phosphor *Japan. J. Appl. Phys.* **32** L791-L793

[25] Kaneko Y, Morimoto K and Koda T 1982 Optical properties of alkaline-earth chalcogenides. I. Single crystal growth and infrared reflection spectra due to optical phonons *J. Phys. Soc. Japan* **51** 2247-54

[26] Caurant D, Gourier D, Demoncy N, Ronot I and Tham-Thi M 1995 Paramagnetic defects induced by mechanical stress in calcium sulfide phosphor *J. Appl. Phys.* **78** 878-92

[27] Spencer J N, Merrikin D, Pope S J A, Morgan D J, Carthey N and Murphy M 2020 CW EPR investigation of red-emitting CaS:Eu phosphors: rationalization of local electronic structure *Adv. Opt. Mater.* **8** 2001241

[28] Ghosh P K and Pandey R 1982 Thermoluminescence due to intrinsic point defects in polycrystalline calcium sulphide *J. Phys. C: Solid State Phys.* **15** 5875-85

[29] Dieke G H and Crosswhite H M 1963 The spectra of the doubly and triply ionized rare earths *Appl. Opt.* **2** 675-86

[30] Scott B P, Zhao F, Chang R S F and Djeu N 1993 Upconversion-pumped blue laser in Tm:YAG *Opt. Lett.* **18** 113-5

[31] Rapaport A, Milliez J, Szipőcs F, Bass M, Cassanho A and Jenssen H 2004 Properties of a new, efficient, blue-emitting material for applications in upconversion displays: Yb, Tm: KY_3F_{10} *Appl. Opt.* **43** 6477-80

[32] Güell F, Mateos X, Gavaldà J, Sole R, Aguiló M, Dıaz F and Massons J 2004 Blue luminescence in Tm^{3+}-doped $KGd\,(WO_4)_2$ single crystals *J. Lumin.* **106** 109-14

[33] Li S, Wand L Tang D, Cho Y, Liu X, Zhou X, Lu L, Zhang L, Takeda T, Hirosaki N and Xie R-J 2018 Achieving high quantum efficiency narrow-band β-sialon:Eu^{2+} phosphors for high-brightness LCD backlights by reducing the Eu^{3+} luminescence killer *Chem. Mater.* **30** 494-505

Figure captions

Figure 1. Powder X-ray diffraction patterns of CaS:Eu^{2+}, Tm^{3+}. The concentrations of Eu and Tm are shown. The patterns of the powder diffraction files of CaS and Tm$_2$O$_3$ are also provided.

Figure 2. Diffuse reflectance spectra of CaS:Eu^{2+}, Tm^{3+} with different Eu and Tm concentrations at 300 K.

Figure 3. (a) Internal quantum efficiency plotted against the concentration of Eu^{2+} in CaS:Eu^{2+}, Tm^{3+} (Tm=2%). (b) Eu concentration dependence of the TL peak intensity at 270 K and the afterglow time.

Figure 4. TR-F spectra and decay curves of CaS, CaS:Eu=0%, Tm=0% and CaS:Eu=0%, Tm=2% in the nanosecond time range at 15 K. In (a), the TR-F spectra are shown while the laser excites the samples (the sampling time of 50 ns). Stray light of the second harmonics of the excitation Nd:YAG laser is shown at 532 nm. In (b), initial decay profiles are shown (the sampling time of 1 ns and the measurement wavelength of 420 nm). The laser profile is also included.

Figure 5. TR-F spectra and decay curves of CaS:Eu=0%, Tm=0% and CaS:Eu=0%, Tm=2% in the millisecond time range (the sampling time of 0.05 ms) at 15 K. In (a), TR-F spectra obtained at 0.5 ms after the laser excitation are shown. In (b), luminescence intensities at 420 nm are plotted against 0–10 ms.

Figure 6. TR-F spectra and decay curves of CaS:Eu=0.1%, Tm=0% and CaS:Eu=0.1%, Tm=2% in the nanosecond time range at 15 K. In (a), TR-F spectra are shown while the laser excites the samples (the sampling time of 50 ns). Stray light of the second harmonics of the excitation Nd:YAG laser is shown at 532 nm. Marks above the 650-nm red emission band show phonon shifts (280 cm^{-1}) from the zero phonon line at 625 nm (see figure S3). In (b), initial decay profiles of the 650-nm red emission and the 420-nm blue emission are shown (the sampling time of 1 ns). The laser profile is also included.

Figure 7. TR-F spectra and decay curves of CaS:Eu=0.1%, Tm=0% and CaS:Eu=0.1%, Tm=2% in the millisecond time range at 15 K. In (a), TR-F spectra obtained at 0.5 ms after the laser excitation are shown. Marks above the 650-nm red emission band show phonon shifts (280 cm^{-1}) from the zero phonon line at 625 nm (see figure S3). In (b), luminescence intensities of the 650-nm emission and the 420-nm blue emission are shown (the sampling time of 0.05 ms). The dashed line shows the background of this measurement.

Figure 8. (a) TR-F spectra of CaS:Eu=0.01%–1%, Tm=2% obtained while the laser excites the samples (the sampling time of 50 ns). Stray light of the second harmonics of the excitation laser is shown at 532 nm. The measurement temperature is 15 K. (b) Emission decay characteristics of CaS:Eu=0.01%, Tm=2% at 650 and 420 nm. (c) Emission decay characteristics of CaS:Eu=1%, Tm=2% at 650 and 420 nm. For (b) and (c), the emission intensity is normalized by the intensity at the time origin. The sampling time is 50 ns.

Figure 9. Temperature changes of the TR-F spectra of CaS:Eu^{2+}=0.01%, Tm^{3+} =2%. The spectra are obtained while the laser excites the samples. The sampling time is prolonged to 500 ns and the measured emission intensity becomes larger compared to that in figure 8(a). Stray light relevant to the excitation laser is not recognized.

Figure 10. Temperature dependences of the initial intensity at 420 and 650 nm (the sampling time of 500 ns) for CaS:Eu^{2+}=0.01%, Tm^{3+} =2%.

Figure 11. Decay curves at 650 and 420 nm (the sampling time of 0.05 ms) for CaS:Eu^{2+}=0.1%, Tm^{3+} =2%. The temperature is 15 K (open symbols) or 300 K (closed symbols).

Figure 12. TL glow curves of CaS:Eu^{2+}, Tm^{3+}. The concentrations of Eu^{2+} and Tm^{3+} are shown. Glow curves for CaS:Eu=0.1%, Tm=0% and CaS:Eu=0.1%, Tm=2% are shown in reduced form to compare peak temperatures. The heating rate is 5 K min^{-1}, and the voltage of the photomultiplier tube (PMT) is kept constant at 580 V.

Figure 13. Schematic electronic structure model of CaS:Eu^{2+}, Tm^{3+}. The band gap from the valence band (VB) to the conduction band (CB) is drawn as 5.3 eV. The electron trap depth of 0.3 eV was obtained from the TL measurement [16]. (a) Laser excitation, (b) levels related to Tm^{3+}, (c) defect levels due to the sulfur vacancy of the host crystal (V$_S$), (d) levels related to Eu^{2+}, and (e) the interaction between V$_S$ and Eu^{2+}. In (e), electrons trapped in V$_S$ slowly move to Eu^{2+}, which is the origin of the afterglow.
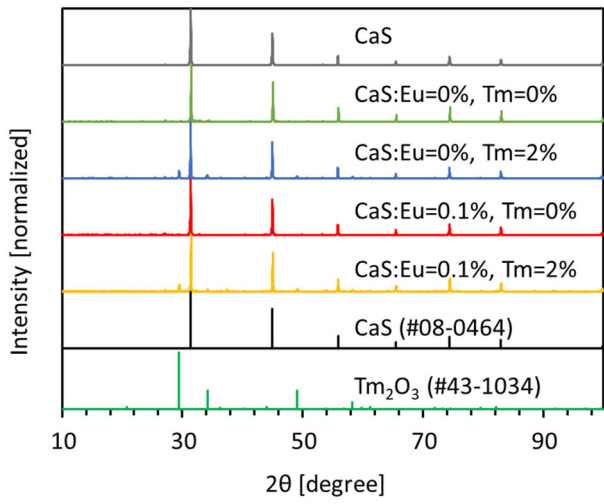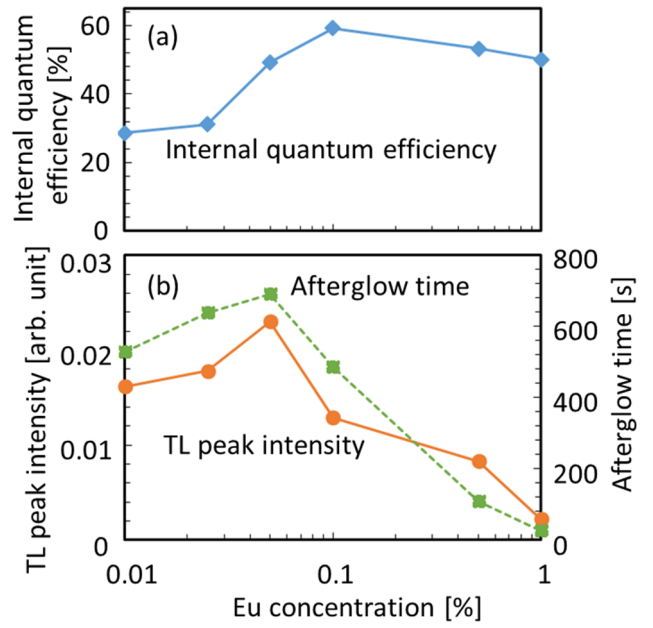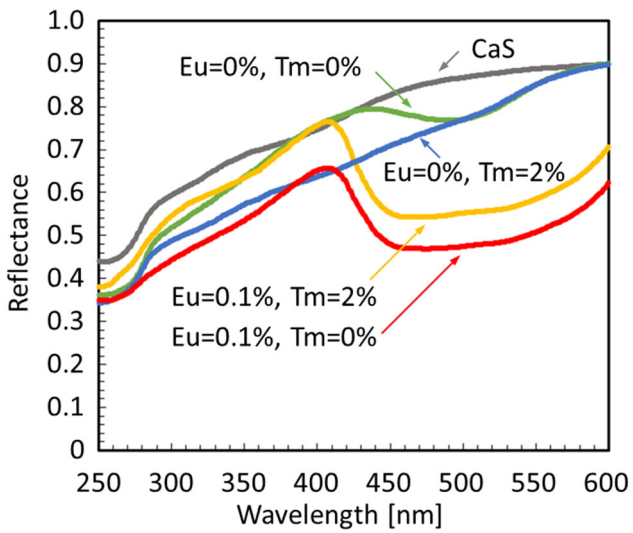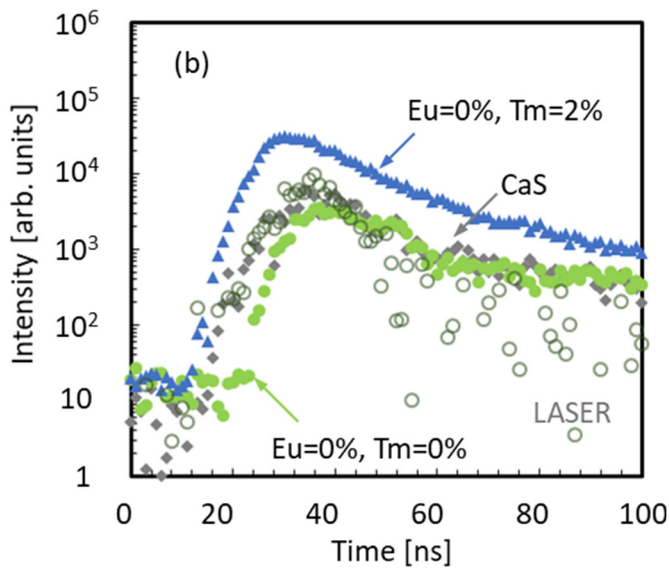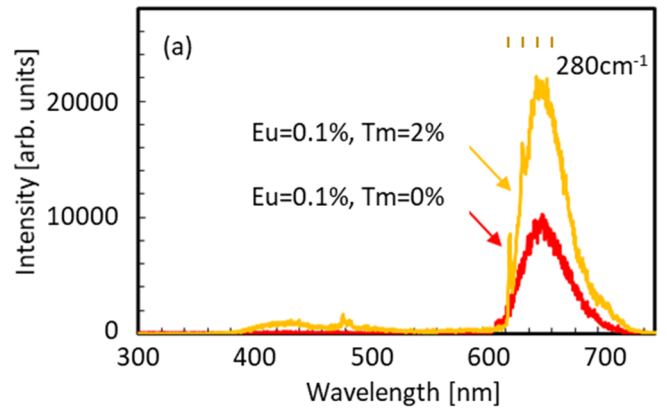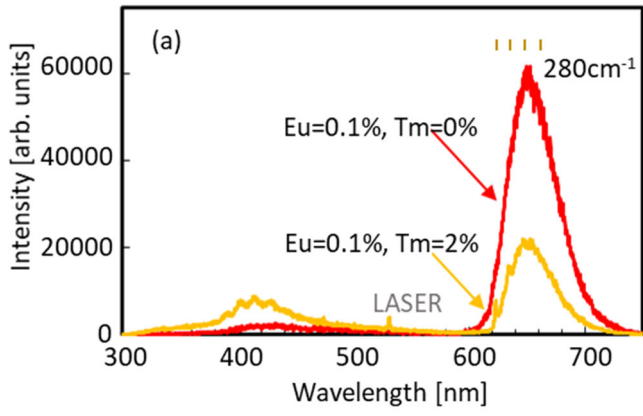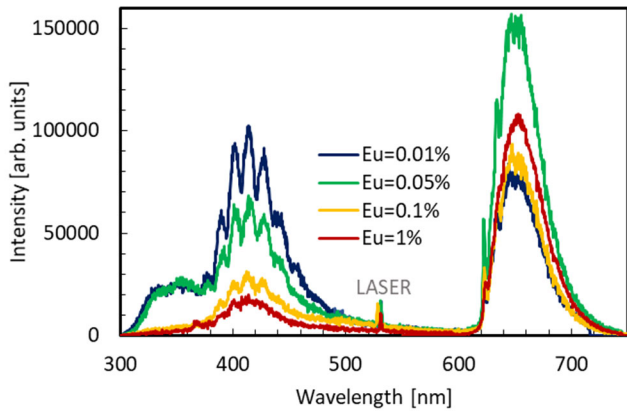
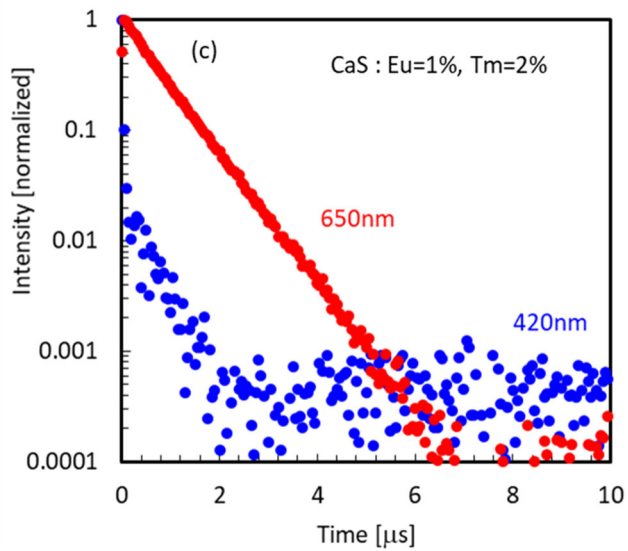Figures

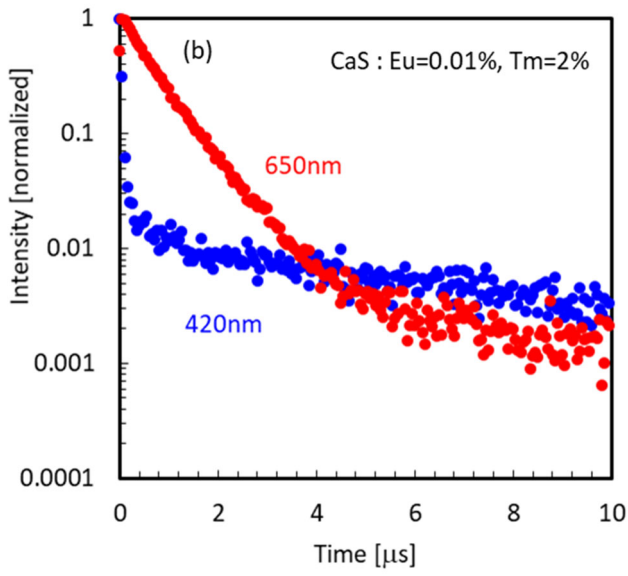Figure 1

Figure 3

Figure 2
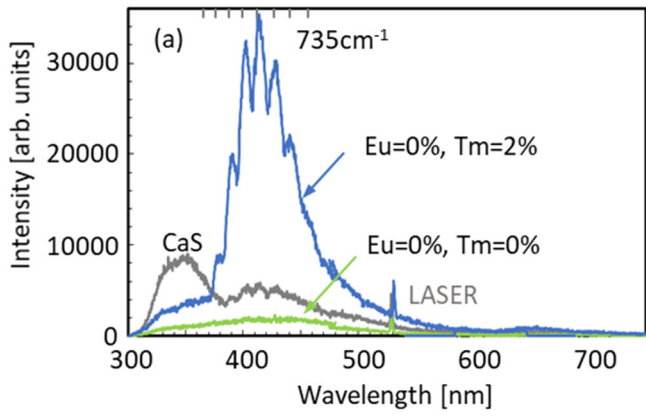
Figure 4
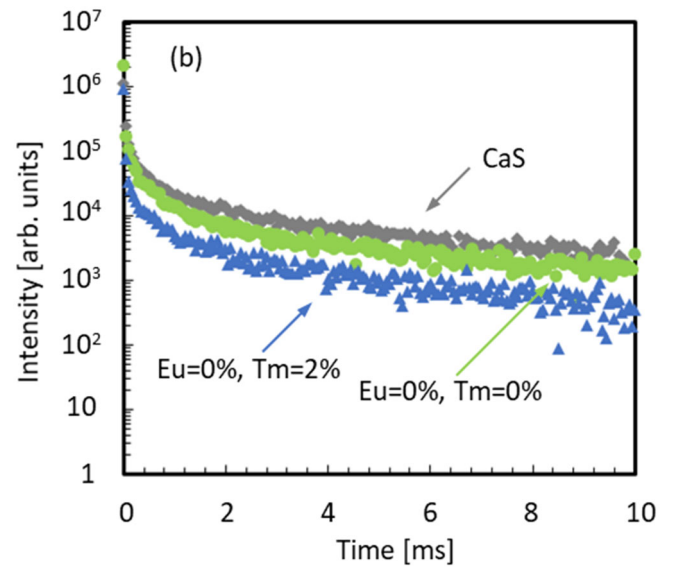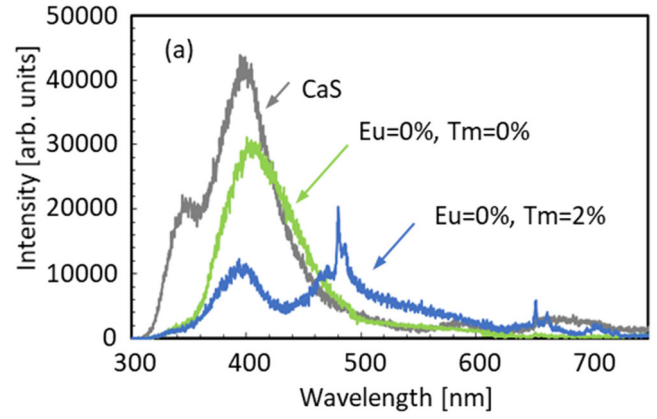
Figure 5
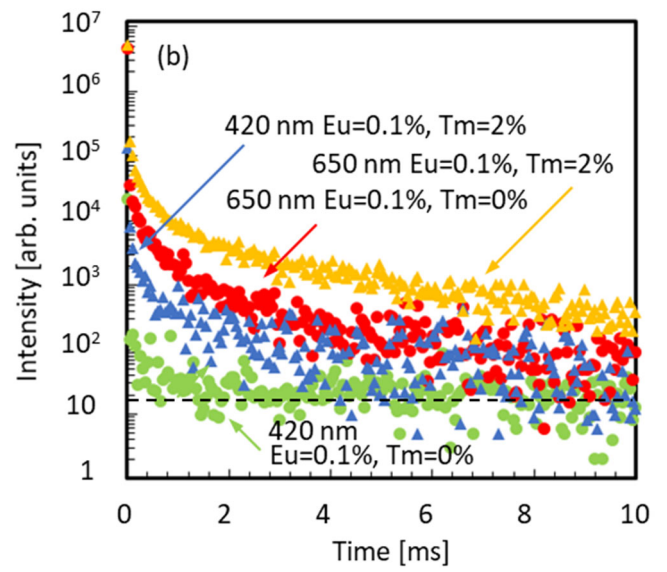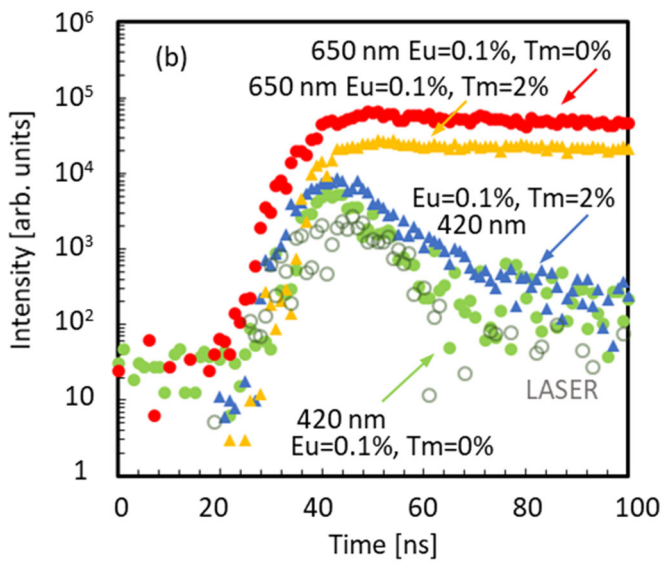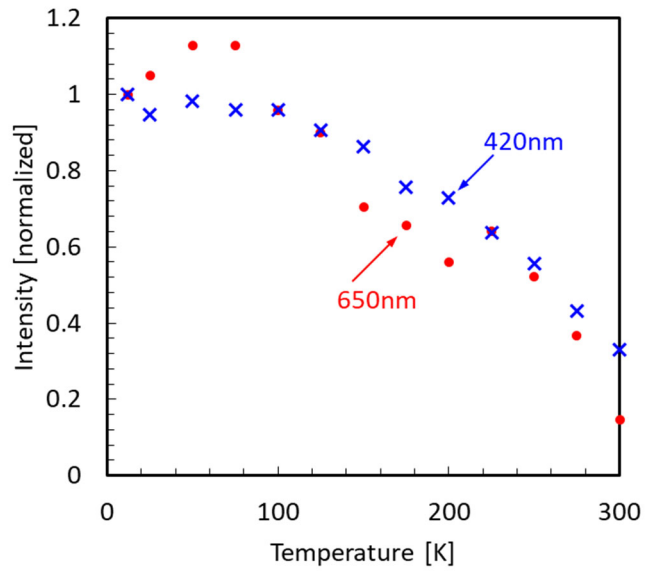
Figure 6

Figure 7
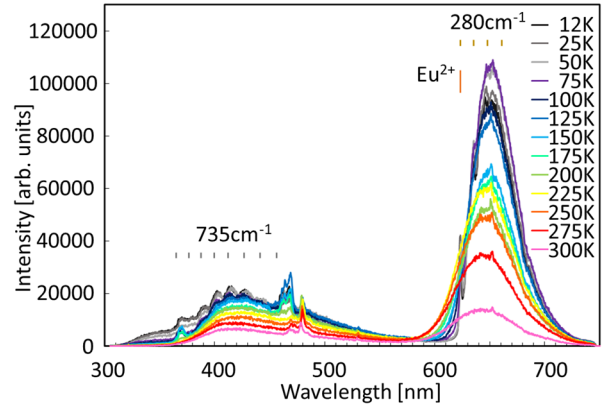
Figure 9

Figure 10
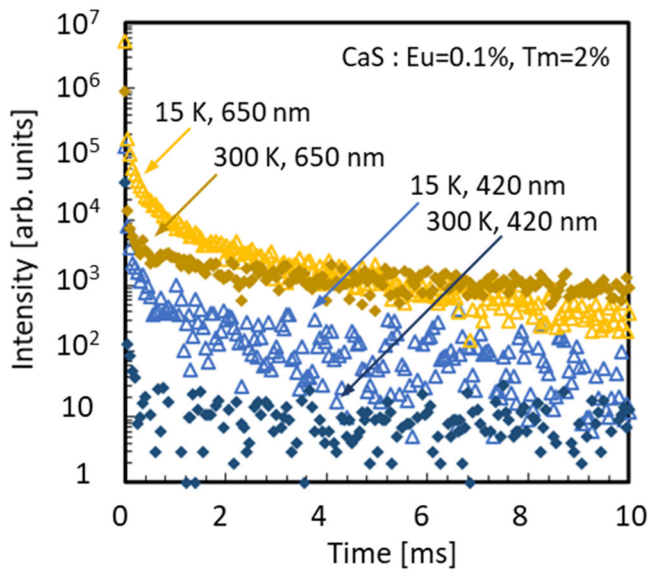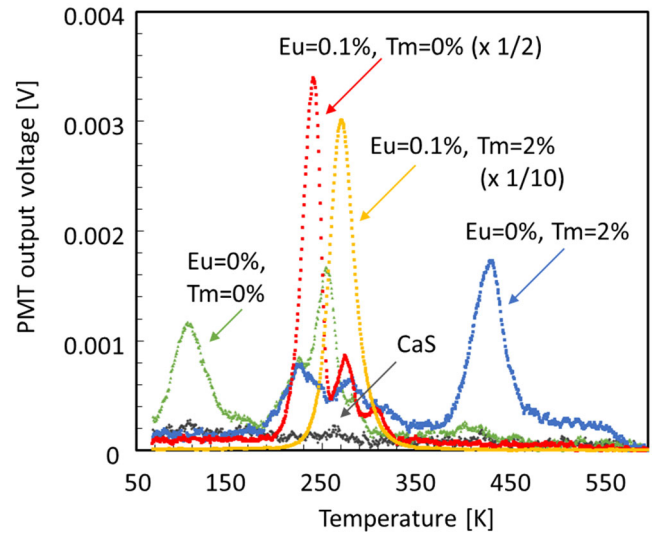
Figure 8

Figure 11

Figure 12
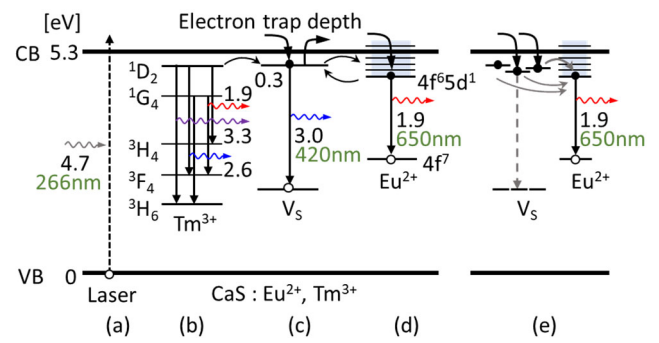
Figure 13

Red afterglow and luminescence arising from defects in CaS:Eu^{2+}, Tm^{3+}

Yoriko Suda[1,2], Yuki Tamura[2], Syota Yamaguchi[2], Yasushi Nanai[3] and Tsuyoshi Okuno[2]

[1] Department of Engineering, Tokyo University of Technology, Hachioji, Tokyo 192-0982, Japan

[2] Department of Engineering Science, The University of Electro-Communications, Chofu, Tokyo 182-8585, Japan

[3] Department of Materials Science and Engineering, National Defense Academy, Yokosuka, Kanagawa 239-8686, Japan

E-mail: h57924d8@edu.teu.ac.jp, sudayoriko@uec.ac.jp

SUPPLEMENTARY MATERIALS

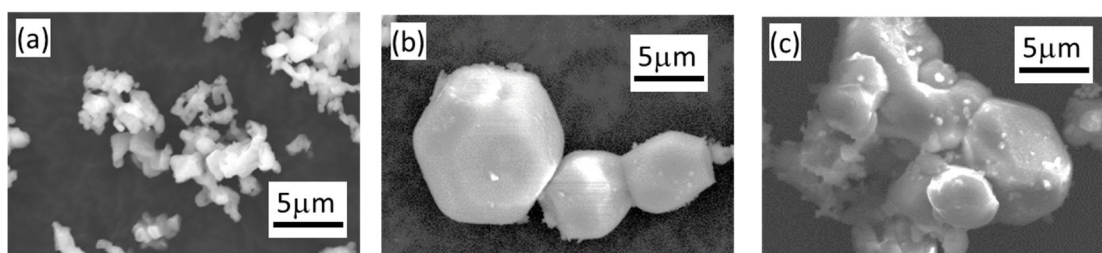### 1. Scanning electron microscope images

Figure S1. Scanning electron microscope (SEM) images of CaS phosphors. The secondary electron image is observed at 15 kV using JSM-6510LV (JEOL Ltd., Japan). (a) CaS, the raw material as is purchased, includes small particles of less than 0.5 μm. (b) Well-formed crystals with the size of 5-10 μm are observed for CaS:Eu=0%, Tm=0% (heat-treated). (c) For CaS:Eu=0.01%, Tm=2%, particles with the similar size to that in (b) are shown, and are aggregated. The particle is enlarged by the heat treatment in (b) and (c). It is assumed that the number of defects on the surfaces is not increased by the heat treatment. We consider that the surface effects are not discussed in this paper. A high resolution transmission electron microscope with selected-area electron diffraction capability should be used to characterize the surface defects. Such study is left for future research.
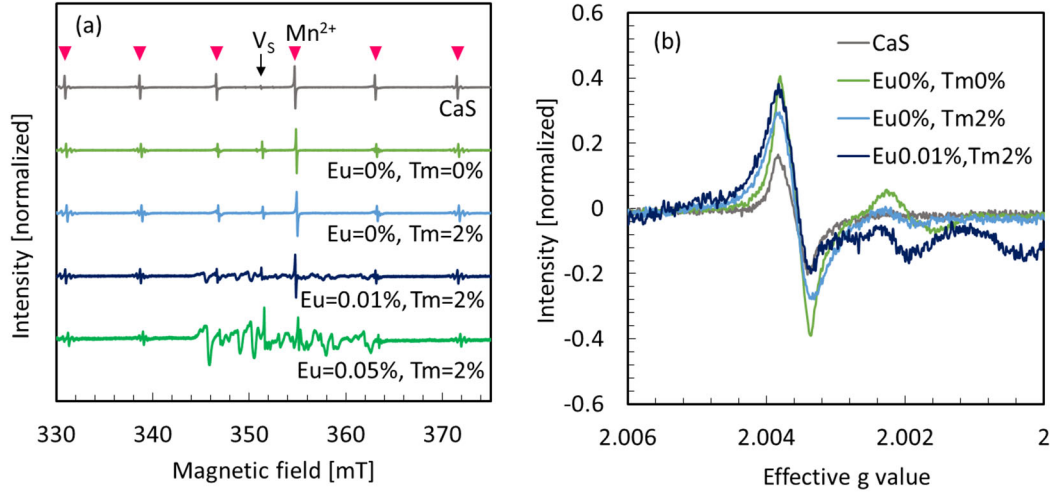
2. Electron paramagnetic resonance spectra

Figure S2. Electron paramagnetic resonance (EPR) (E500-10/12, Bruker, MA, USA) spectra at 300 K for CaS:Eu, Tm. The resonant microwave frequency is 9.85 GHz, and the microwave power is 2 μW. The spectra of CaS, CaS:Eu=0%, Tm0%, CaS:Eu=0%, Tm=2%, CaS:Eu=0.01%, Tm=2% and CaS:Eu=0.05%, Tm=2% are shown in (a). The six structures indicated by the down triangles are due to natural impurities of Mn^{2+} unavoidable in Ca^{2+} [1, 2]. The signal due to sulfur defects (V_S) is located near 352 mT (g = 2.003) [2]. The EPR intensity is normalized by the Mn^{2+} signal at 355 mT close to V_S, considering that the intensity of Mn^{2+} does not change by the heat treatment. For CaS:Eu=0.01%, Tm=2% and CaS:Eu=0.05%, Tm=2%, complicated signals from Eu^{2+} [1, 2] appear at 345-365 mT. In the spectra of CaS:Eu=0.05%, Tm=2% and other samples (not shown in the figure) with higher Eu concentrations, the signals from Eu^{2+} and that of V_S are overlapped. It is not possible to evaluate the signal intensity of V_S for the samples with the high Eu concentrations. In (b), the region of the V_S signal near 352 mT (g=2.003) is expanded. The horizontal axis is converted to the g value. The V_S signal intensities do not change so much among the four samples (less than twice). It is assumed that the defects responsible for the V_S signal do not change by the heat treatment or the doping of Eu^{2+} or Tm^{3+}. The interaction between the defect states and Eu^{2+} is discussed in this paper.
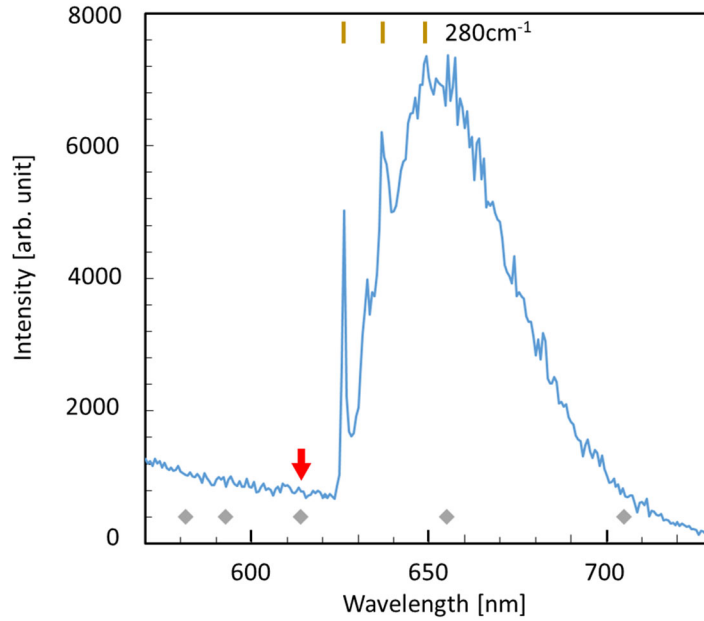
3. Photoluminescence spectrum

Figure S3. Photoluminescence spectrum of CaS:Eu=0.1%, Tm=0% at 15 K. The excitation light source is a Xe arc lamp (300 W), and a photomultiplier tube (R928, Hamamatsu Photonics, Japan) is used for detection. In some of the references [2-4] on CaS:Eu^{2+} phosphors, emission from Eu^{3+} was reported. Eu^{3+} in CaS:Eu^{2+} may affect the optical properties of Eu^{2+} in CaS. The excitation wavelength is set to be 370 nm, which is suitable for observing the emission of Eu^{3+} [2-4]. If Eu^{3+} is present in this sample, a strong emission peak arising from the intra 4f^6-4f^6 transition of $^5D_0$-$^7F_2$ in Eu^{3+} would have appeared at 614 nm (the arrow). The other emission peaks would also have appeared at wavelengths indicated by gray diamonds. However, no emission peak is present at these wavelengths. No emission of Eu^{3+} is found also under the excitation at 390 nm (the transition of $^7F_0$-$^5D_4$ in Eu^{3+}), and this is the same in any CaS:Eu,Tm sample in this paper. It is concluded that no Eu^{3+} is present and Eu^{3+} is not considered in this paper.

The narrow strong peak at 625 nm is the zero phonon line, and some fine structures in the longer wavelength region are phonon shifts (280 cm^{-1}). These structures are the same as those reported for CaS:Eu^{2+}, Na$^+$ [3]. This phonon shift is an average value of the vertical and horizontal phonon energies (229 and 342 cm^{-1}, respectively) of the host crystal CaS [3]. This phonon shift is repeated periodically (marked lines in the figure as well as in figures 6(a) and 7(a)).

REFERENCES

[1] Caurant D, Gourier D, Demoncy N, Ronot I and Tham-Thi M 1995 Paramagnetic defects induced by mechanical stress in calcium sulfide phosphor *J. Appl. Phys.* **78** 876-892

[2] Spencer J N, Merrikin D, Pope S J A, Morgan D J, Carthey N and Murphy M 2020 CW EPR investigation of red-emitting CaS: Eu phosphors: rationalization of local electronic structure *Adv. Opt. Mater.* **8** 2001241

[3] Yamashita N, Fukumoto S, Ibuki S and Ohnishi H 1993 Photoluminescence of Eu^{2+} and Eu^{3+} centers in CaS: Eu, Na phosphors *Japan. J. Appl. Phys.* **32** 3135-9.

[4] Fukumoto S, Hayashi Y, Ibuki S, Abe K and Ohnishi H 1993 Photoluminescence of Eu^{3+} in CaS: Eu phosphor *Japan. J. Appl. Phys.* **32** L791-L793